POLITECNICO DI TORINO
Repository ISTITUZIONALE

Sustainable freshwater production using passive membrane distillation and waste heat recovery from portable generator sets

(Article begins on next page)

28 April 2024

Sustainable freshwater production using passive membrane distillation and waste heat recovery from portable generator sets

Matteo Morciano[a,b,*], Matteo Fasano[a,*], Luca Bergamasco[a], Alessandro Albiero[a], Mario Lo Curzio[a], Pietro Asinari[a,b], Eliodoro Chiavazzo[a,**]

[a]*Department of Energy, Politecnico di Torino, Corso Duca degli Abruzzi 24, 10129 Torino, Italy*
[b]*Clean Water Center, Politecnico di Torino, Corso Duca degli Abruzzi 24, 10129 Torino, Italy*

Abstract

More than two billion people live in areas affected by water stress. In some coastal regions, freshwater supply has been progressively improved by large-scale desalination systems, which are nowadays mostly driven by non-renewable energy sources. Here we discuss, and experimentally investigate, the use of small-scale desalination devices for freshwater production powered by waste heat from electric power generators. The water purification technology relies on a passive, multi-stage and thermally-driven membrane distillation device, recently proposed by some of the authors of this work. The distiller is powered by low-grade (temperature lower than 80°C) waste heat, recovered from the coolant circuit of small diesel engines for electricity production. Field experiments show that, for the tested engine, up to 1.12 kW m^{-2} can be recovered in standard operating conditions, which yield a nearly 2.61 L m^{-2} h^{-1} freshwater production from seawater. A lumped parameter model, validated by experiments, shows that this productivity could be eventually enhanced by tuning the number of distillation stages. Utilization with exhaust gases, and thus higher feeding working temperatures, is also discussed. The proposed solution may provide a sustainable, simple, inexpensive and efficient means for freshwater production from recovered waste heat, which would otherwise be wasted to the ambient. Therefore it could be particularly effective, for instance, for field hospitals in remote or impoverished areas, especially in emergency situations.

Keywords: Desalination, Membrane distillation, Waste heat recovery, Low-grade heat, Sustainability

1. Introduction

As of today, more than two billion people worldwide live in regions suffering severe water stress, and nearly four billions experience water scarcity for at least one month every year. Three people out of ten lack direct access to safe drinkable water, and almost half of the people that are drinking water from unprotected sources live in the Sub-Saharan Africa. The global water demand is expected to increase up to 30% by 2050, owing to the population growth - more than half of which (1.3 out of 2.2 billion globally) is expected in Africa [1]. For these reasons, reduced access to freshwater and chronic water shortages are considered among the most important global risks for society, especially in developing countries and emerging economies [2, 3].

The daily basic requirement of clean water is recommended as 50 liters per person, including drinking water (2 liters), sanitation services, hygiene and cooking [4]. This minimum requirement is unmet especially in remote areas in impoverished or developing countries [5], where infrastructures for the distribution of water lack. In those cases where contaminated or salty water sources and electricity are available, active desalination and purification technologies may be a solution [6, 7]; however, they may be not feasible or economically convenient in areas with poor or no connection to the electric power grid (*i.e.* off-grid) [8, 9]. In this sense, passive distillation technologies - which are capable to operate without any mechanical moving part thus requiring low capital and maintenance cost [10], may represent an important alternative. A broad variety of passive desalination approaches has been developed in the recent years, based for example on heat localization [11, 12], nanophotonics-enabled membrane distillation [13, 14] or hybrid photovoltaic-thermal sys-

*Equal contributors
**Corresponding author: eliodoro.chiavazzo@polito.it

tems [15]. However, the productivity of passive desalination technologies, which is generally lower than the active ones, represents a limit for their widespread adoption and utilization [16, 17].

A completely passive and highly-efficient solution for water distillation has been presented, extensively studied and discussed by some of the present authors in a previous work [18]. The proposed device performs a complete distillation process at ambient pressure with efficient energy management, thanks to a series of multiple evaporation and condensation stages (multi-stage concept [19], here adopted for a passive device). The stratigraphy of the stages is indeed designed to recover the latent heat several times before it is lost to the environment, thus increasing the productivity. The water feeding system exploits capillary action, which avoids utilization of any moving mechanical part (which may be subject to aging and possible failure) and thus ancillary energy consumption. Advantages of this solution include: compactness, simplicity, low-cost, little and non-skilled maintenance. In the previous work [18], this device has been tested for operation with solar energy; yet, it can be fed with different sources of low-temperature heat, such as geothermal energy and waste thermal energy.

Thermal desalination technologies using waste heat have received increasing attention during the last years, as the energy recovery contributes to a better energy exploitation and thus to a reduction of the carbon footprint in case of fossil-fuel generated energy. In particular, low-grade heat recovered from industrial processes or from geothermal origin represents a valuable resource for desalination [20–22]. Among all the available thermal desalination technologies [23], Multi-Effect Distillation (MED) is ideal in this sense, and has indeed particularly undergone substantial improvements [24, 25]. However, MED is generally referred to an active technology, and it is thus more suitable for large-scale plants [26].

In this work, we present the original coupling between a completely passive, multi-stage and thermally-driven membrane distillation device with the coolant and/or exhaust-gas circuit of small diesel engines for electric power generation. These latter generators are typically used to guarantee continuity of the electrical supply to field hospitals in remote areas in emergency situations, yet not only. These engines usually present an electricity generation efficiency of around 40%, with a considerable part of energy lost to the environment as waste heat. Nearly 30% of this thermal energy is wasted through the exhaust gases, around 25% is dissipated in the coolant circuit while the remaining 5%

through other heat losses [27]. The main idea in this work is that part of this wasted thermal energy can be recovered and used to produce freshwater from salt and/or brackish water, either from the coolant circuit and/or from the exhaust gases. Here we focus on the heat recovery from the coolant circuit, where the working temperature of the glycol-water mixture is typically lower than 80°C. In fact, low-grade heat is particularly suitable to power membrane distillation systems such as the proposed compact distiller, which presents the desirable feature of working at low temperatures. Even though some solutions for thermal desalination using waste heat recovery from electric power generators have already been proposed [28], to the best of our knowledge, this represents the first realization using a completely passive, self-operating desalination device based on multi-stage membrane distillation.

The article is organized as follows. In Section 2, we present and discuss the experimental set-up, together with a detailed description of the working principles of the waste heat recovery and membrane distillation systems. In Section 3, a theoretical model for the desalination device and resulting clean water production is presented. Section 4 focuses on the discussion of the experimental and modeling results, along with a comparison of the productivity of the proposed solution with others available in the literature. Finally, the conclusions are drawn in Section 5, where an outlook on practical applications and future perspectives are given.

2. Materials and methods

2.1. Experimental set-up

The set-up used for the experimental tests is shown in Fig. 1. The electric power generator set (labeled as GENSET) and the low temperature, passive and multi-effect membrane desalination device (labeled as LT-MD) are thermally coupled through a waste heat recovery system (heat exchanger, labeled as HEX) engineered at Politecnico di Torino. The waste heat is extracted from the cooling circuit of the generator set and used to power the LT-MD device (in thermal contact with the heat exchanger), thus enabling a thermal gradient across the latter.

The used generator set is a FG Wilson F9.5-1 with a 4-stroke diesel engine and an electrical power output of 8.5 kVA / 6.8 kW (prime) and 9.5 kVA / 7.6 kW (standby) at 50 Hz. The generator set is equipped with an adjustable resistive load, which allows to study the desalination prototype under different operating conditions: no load, half load (3 kW) and full load (6 kW). The
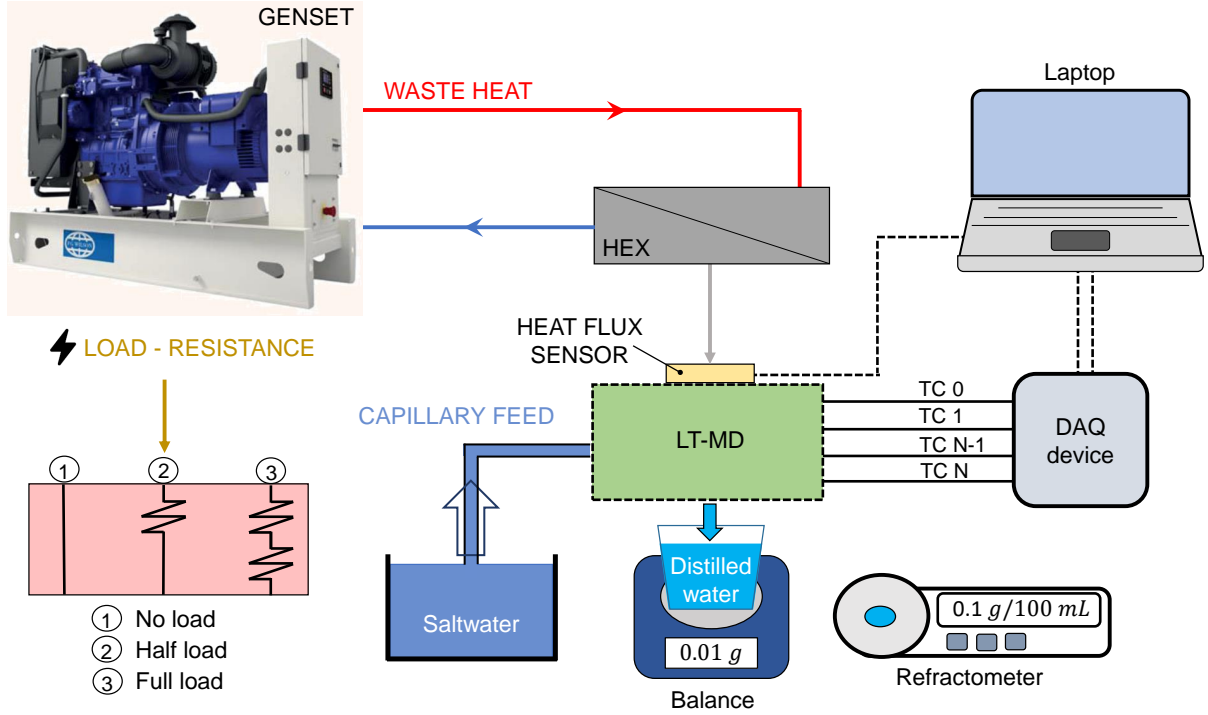
Figure 1: Experimental set-up used for testing the performance of the multi-stage membrane distillation device developed at Politecnico di Torino and powered by the waste heat recovered from the coolant circuit of an emergency power generator. The following components are used for the experimental tests, carried out in field conditions: a laptop for data storage and elaboration, a data acquisition board (DAQ device), a digital refractometer for the measurement of water salinity, a balance for measurement of the output distilled water, an output basin for collecting the distilled water, an input basin for supplying the salt water, the modular distiller (LT-MD), the generator set (GENSET) and the heat exchanger (HEX). The GENSET can operate at either half or full working conditions, thanks to a tunable electrical resistance employed to simulate an electric load. The DAQ system is employed to monitor the temperature in the LT-MD device by means of the thermocouples (TC).

cooling fluid of the thermal engine consists of a water-glycol mixture, which flows at temperatures lower than 80°C and is used to provide the thermal energy to the desalination process, which needs a thermal gradient to operate. In fact, the distiller relies on a membrane distillation process operated in multiple stages, where the driving force is the difference in vapor pressure between salt and distilled water, which depends on temperature and salinity (see the next Section for details). An advantage of this distillation process is the relatively low operating temperature required ($< 80°C$), which conveniently suits the possibility of using low-grade waste heat from the electric power generator.

The thermal power recovered by the heat exchanger is experimentally measured using a heat flux sensor (gSKIN XP 26 9C, GreenTEG). The heat flux sensor is positioned between the bottom aluminum cover of the heat exchanger and the top surface of the LT-MD device. When a thermal flux passes through the sensor, the transducer produces an electrical signal; thus, the heat flux per unit surface is obtained as $\phi = U/S$, being U the output voltage [μV] and S the temperature-corrected sensitivity of the sensor [$\mu V \, (Wm^{-2})^{-1}$].

The salinity of the input salt water and produced freshwater, is measured using a digital refractometer (HI 96821; Hanna Instruments; accuracy $\pm$ 0.2% and resolution 1 $g \, L^{-1}$) is adopted. The inlet and outlet water basins (1 L capacity) are used to gather the processed salt water and the distilled one. A precision balance (Kern PCB 1000-2; 0.01 g resolution) is used to weigh the distilled water basin, in order to monitor its mass variation with time. Several thermocouples (RS Pro; K-type [29]) connected to a data acquisition board (DAQ, National Instruments) are installed. Thermocouples are placed in each stage of the distiller, in contact with the evaporator and condenser wicks (more details in the next Section).
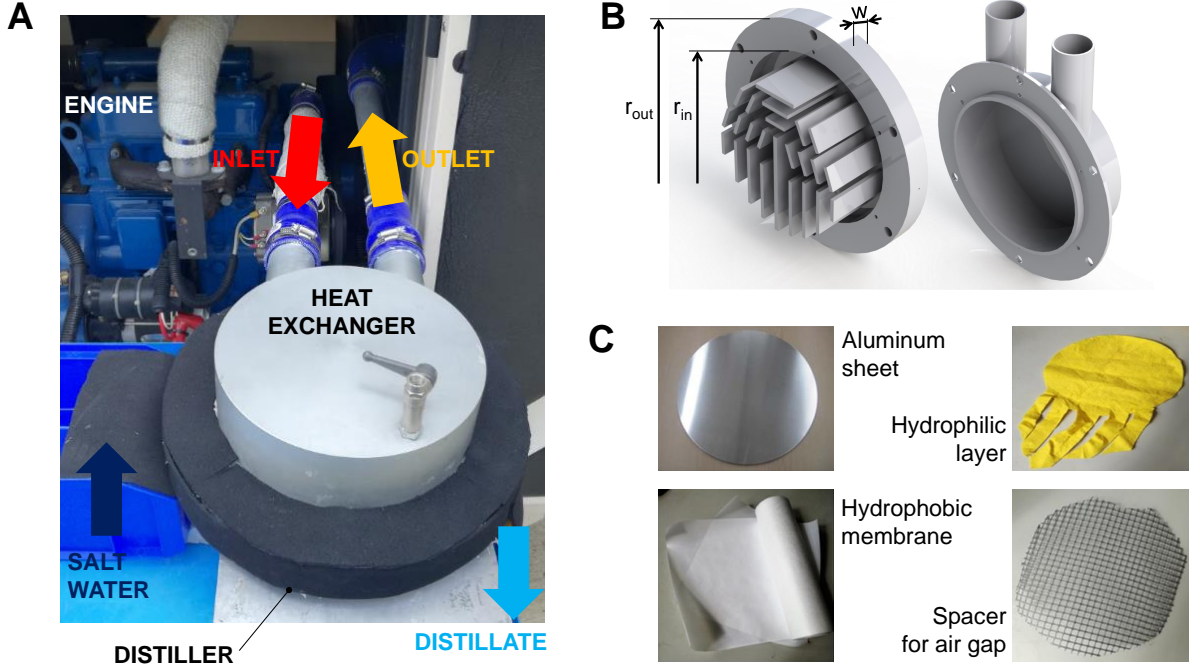
3

Figure 2: Experimental implementation of the passive distillation system powered by the coolant circuit of an electricity generator set. (A) Coupling of the compact desalination device with the waste heat recovery system developed at Politecnico di Torino. Note that the distillation device is placed on the bottom side of the heat exchanger. (B) Details of the in-house designed heat exchanger for heat recovery from the coolant circuit of the electric power generator. (C) Pictures of the employed aluminum sheet, hydrophilic layer, hydrophobic membrane and plastic spacer (adopted to keep an air gap between the membrane and condenser) of the tested 3-stage distiller.

2.2. Details on the waste heat recovery system and desalination device

The waste heat recovery system coupled with the compact desalination device is shown in Fig. 2A, where the heat exchanger is inserted upstream with respect to the radiator of the engine. The heat exchanger was in-house designed to enhance the heat transfer rate using a finned body (Fig. 2B), while limiting the pressure drop between the inlet and outlet sections. The cooling fluid flows across the finned surface at temperatures lower than 80°C, and the measured temperature difference between the inlet and outlet tubes ranges between 1 to 2°C, depending on the operating conditions. The internal and external radii of the plates of the heat exchanger are r_{in} = 104 mm and r_{out} = 150 mm respectively, while the thickness of the base is w = 8 mm. The heat exchanger is made of 7075 aluminum alloy (Ergal7075), which presents a thermal conductivity of 155 W m^{-1} K^{-1}.

The desalination device relies on a tailored stratigraphy (see Fig. 2C and 3), which enables latent heat recovery through a series of multiple evaporation and condensation stages, thus increasing the freshwater productiv-ity. Each stage consists of: two hydrophilic wicks (70% viscous fibers, 18% polypropylene and 12% polyester, with an average area of 0.049 m^2 per wick and 1 mm thickness), which act respectively as evaporators and condensers; a hydrophobic membrane (polytetrafluoroethylene by *ANOW microfiltration*, with an area of 0.067 m^2 per membrane, 150 μm thickness and 0.1 μm average pore radius); an air gap provided by a spacer (1 mm thick porous polypropylene frame); an aluminum plate (1.3 mm thick). Each evaporator is fed via capillary effect through the wick strips, which are immersed in the salt water basin; each condenser, instead, discharges by gravity the produced distillate through a strip immersed in the distilled water basin (compare Fig. 1). It is worth to remark that the scope of the spacers (air gaps) is to increase the distillation performance (see Section 4) and to prevent damaging of the membranes.

The driving force of the process is the different vapor pressure between the evaporators and condensers, which depends on temperature and salinity differences across each stage. The whole process is sustained by the heat entering the top HEX surface, which induces the first vapor formation in the upper evaporator layer. Only
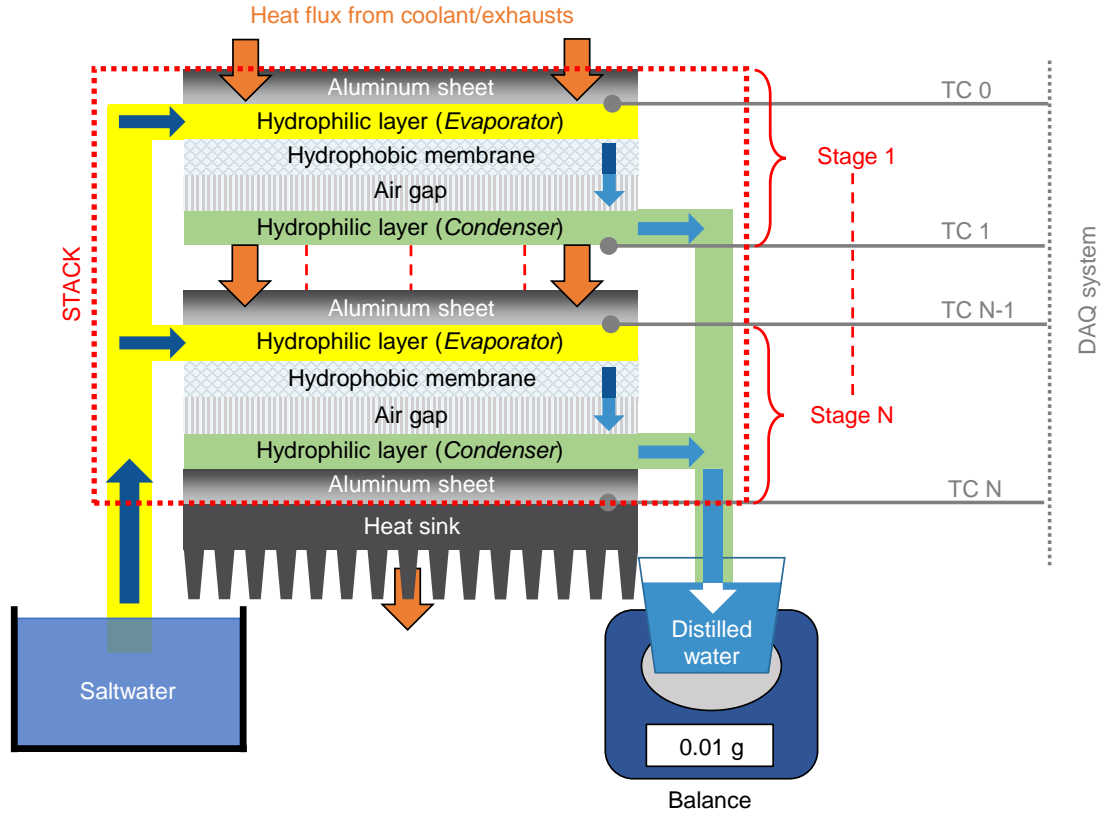
Figure 3: Stratigraphy and multi-stage working principle of the distiller, to produce freshwater from salt water. In the tested case, the device consists of three identical stages of distillation. Each stage is made of an aluminum sheet, a hydrophilic layer acting as evaporator, a hydrophobic membrane, an air gap obtained with the use of a plastic spacer and a hydrophilic layer acting as condenser. Salt water is supplied to evaporators by capillarity; freshwater is released by gravity. The produced distilled water is monitored by means of a precision balance. The temperature profile through the multiple stages of distillation is measured by thermocouples (TC N) attached to the aluminum sheets, and their signal is elaborated by a Data Acquisition (DAQ) system. The thermal energy required for the distillation processes is supplied by the coolant circuit of the internal combustion engine via the heat exchanger; after the multiple distillation process, heat is discharged back into the environment at lower temperature via a heat sink.

water vapor can flow across the hydrophobic membrane, while the salt and liquid phase of water remain on the upper side of the membrane. The water vapor condenses on the wick underneath the membrane (condenser) and, due to gravity, distilled water drains out through the strips in the freshwater basin. The released latent heat during condensation becomes available to drive the next distillation stage, where the same process occurs. This is possible thanks to the high thermal conductivity of the thin aluminum plate, placed between the condenser and the evaporator of the next stage. At the bottom of the whole stack, an aluminum heat sink (ABL components, 0.07 K W^{-1} thermal resistance) promotes heat rejection at the lowest temperature towards the environment, thus favoring condensation in the last stage. The described

device has been operated under natural convection without requiring any additional power supply for cooling purposes.

3. Lumped parameter model

A one-dimensional lumped parameter model is adopted to estimate the vapor flux and the heat transfer through each stage of the distillation device. This model has already been extensively discussed in our previous work [18] for solar-driven desalination; here, we apply it for the analysis of the coupling with the coolant circuit of the electric power generator.

Raoult's law is considered to evaluate the vapor pressure gradient between the salt water contained in the

upper hydrophilic layer (evaporator) and the freshwater in the lower hydrophilic layer (condenser) in each stage [30–32], namely:

$$\Delta p_v = a(Y_E)p_v(T_E) - a(Y_C)p_v(T_C);\qquad(1)$$

where a is the activity of water, which considers the salinity of the solution; Y_E and Y_C are the mass fractions of salt in the feed and distilled solution ($Y = m_{salt}/m_{sol}$), respectively; p_v is the vapor pressure of water; T_E and T_C are the temperatures of the feed and distilled solutions, respectively [33]. Under the assumption of ideal conditions, the activity of an aqueous solution of sodium chloride (NaCl) can be estimated as

$$a = \frac{M_{\text{NaCl}}(1-Y)}{M_{\text{NaCl}}(1-Y) + N_{ions}M_{H_2O}Y},\qquad(2)$$

where $N_{ions} = 2$ for NaCl, M_{NaCl} and M_{H_2O} are the molar masses in grams per mole of sodium chloride and water, respectively. In the experiments, the NaCl-water solution to be treated has salinity equal to 35 g L^{-1}, similarly to seawater; thus, $Y_E = 0.035$ and $a(Y_E) \approx 0.98$ according to Eq. (2). For the distilled water, the activity is clearly $a = 1$. The vapor pressure as a function of temperature is evaluated using Antoine's semi-empirical correlation

$$\log(p_v) = A - \frac{B}{C+T},\qquad(3)$$

where p_v is intended in mm Hg, T in Celsius degrees, A, B and C are material-specific constants that in this case are equal to 8.07, 1730.63 and 233.42, respectively [34].

Maxwell-Stefan and Dusty-Gas models are employed to evaluate the specific mass flow rate (J, in kg s^{-1} m^{-2}) of the produced distillate [35–37]. The Maxwell-Stefan model accounts for the chemical potential and molecular diffusion, which depend on the concentration and interaction among the gas molecules, respectively. The Dusty-Gas model accounts for the collisions between gas molecules and pore walls, and for the viscous flow due to the total pressure gradient across the porous medium. Combining these two models, the mass transport through a porous medium can be expressed as:

$$-\frac{x_i}{RT}\frac{d\mu_i}{dz} = \frac{x_i K_v \tau}{\eta_v \epsilon_m D_{iK}}\frac{dP}{dz} + \sum_{j=1;j\neq i}^{n}\left(\frac{x_j N_i - x_i N_j}{\frac{P\epsilon_m D_{ij}}{RT\tau}}\right) + \frac{N_i}{\frac{P\epsilon_m D_{iK}}{RT\tau}};$$
$$(4)$$

where x_i and μ_i are the mole fraction and chemical potential of species i, R is the universal gas constant (8.314

J K^{-1} mol^{-1}), T the absolute temperature, K_v the viscous permeability coefficient, τ and ϵ_m the tortuosity factor and porosity of the membrane, η_v and P the dynamic viscosity and total pressure of the mixture, z the Cartesian coordinate and D_{iK} the Knudsen diffusion coefficient for species i. Moreover, N_i is the molar flux of species i and D_{ij} the diffusion coefficient of species i in j.

The three terms on the right-hand side of Eq. (4) account respectively for the viscous flow, the molecular diffusion and the Knudsen diffusion. It is worth to point out that the viscous flow term is negligible in the proposed device; in fact, no total pressure difference occurs across the membrane. The chemical potential of the water vapor (μ_w), in case of ideal gas assumption, can be written as $\mu_w = \mu_{w,pure} + RT\ln(x_w)$, where the subscripts w and $w,pure$ refer to water and pure water vapor, respectively. Considering a configuration consisting of a membrane (porosity ϵ_m, thickness d_m) and an air gap (porosity ϵ_a, thickness d_a) between the evaporator and condenser, Eq. (4) can be re-organized in two equations: the first applied to the membrane and the second to the air gap, namely

$$-\frac{dx_w}{dz} = \frac{(1-x_w)N_w}{\frac{P\epsilon_m D_{wa}}{TR\tau}} + \frac{N_w}{\frac{P\epsilon_m D_{wK}}{TR\tau}},\qquad(5)$$

$$-\frac{dx_w}{dz} = \frac{(1-x_w)N_w}{\frac{P\epsilon_a D_{wa}}{TR\tau}}.\qquad(6)$$

Then, Eq. (5) and (6) can be respectively integrated within the membrane and air gap domains with proper boundary conditions (see [18] for a thorough discussion), yielding to

$$J = C_1 \ln\left(\frac{1 + \frac{D_{wa}}{D_{wK}} - x_w^0}{1 + \frac{D_{wa}}{D_{wK}} - x_w^E}\right),\qquad(7)$$

$$J = \frac{C_1}{C_2}\ln\left(\frac{1-x_w^C}{1-x_w^0}\right);\qquad(8)$$

being x_w^E the mole fraction of water in the evaporator, x_w^C in the condenser and x_w^0 at the interface between the air gap and the membrane. Considering that the specific mass flow rate of the distillate through the stage is $J = M_{H_2O}N_w$, with M_{H_2O} being the molar mass of water, the integration constants write

$$C_1 = \frac{M_{H_2O}\epsilon_m P D_{wa}}{RT\tau d_m}\qquad(9)$$

$$C_2 = \frac{\epsilon_m d_a}{\tau \epsilon_a d_m},\qquad(10)$$

where D_{wa} is the diffusion coefficient of the water vapor in air, and D_{wK} is the Knudsen diffusion coefficient of

the water vapor. Note that it is possible to empirically estimate $PD_{wa} = 1.19 \times 10^{-4} \, T^{1.75}$ Pa m^2 s^{-1} [38]. The Knudsen diffusion coefficient can be expressed as:

$$D_{wK} = \frac{8r}{3} \sqrt{\frac{RT}{2\pi M_{H_2O}}},\qquad (11)$$

where r is the average pore radius of the membrane. The correlation between tortuosity and porosity of the membrane is modelled by the Mackie–Meares equation as [39, 40]

$$\tau = \frac{(2 - \epsilon_m)^2}{\epsilon_m}. \qquad (12)$$

Given that, under the typical moist-air conditions of interest here, the vapor molar fraction in the air gap is $x_w \ll 1$, Eqs. (7) and (8) can be combined and then linearized (see [18] for details), finally obtaining:

$$J = C_1 \ln\left(\frac{1 + \frac{D_{wa}}{D_{wK}} - x_w^C - \frac{C_2}{C_1}\left(x_w^E - x_w^C\right)KP}{1 + \frac{D_{wa}}{D_{wK}} - x_w^E}\right), \quad (13)$$

where K is the overall permeability coefficient of the membrane and air gap reported in [18]. Equation (13) is the final form of the model to be validated and used in the analyses reported in the next Section.

In each stage of the distiller, the specific heat flux (q, W m^{-2}) between the evaporating and condensing hydrophilic layers is mainly due to heat transfer by conduction and phase change; therefore, we estimate it as

$$q = \frac{k_{e,g}}{d_g}(T_E - T_C) + J\Delta h_{LV} + q_l, \qquad (14)$$

where $k_{e,g}$ is the effective thermal conductivity in the gap, which includes conduction through the spacer and membrane; $d_g = d_a + d_m$ is the thickness of the gap; T_E and T_C are the temperatures of the feed and permeate solution, respectively; J is the specific mass flow rate of water through the gap; Δh_{LV} is the latent heat of vaporization of water; q_l is the specific heat loss through the lateral surface of the stage.

In summary, the inputs of the model are the recovered thermal source, the ambient temperature, the feed water salinity, the material characteristics (thickness, porosity, thermal conductivity of the different layers) and the number of stages in the stack. The outputs are the temperature profile and the heat flux across each stage of the distiller, as well as its distillate productivity.

4. Results and discussion

4.1. Experimental campaign

The experimental campaign is carried out on a three-stage configuration of the distiller, processing a NaCl-water solution with 35 g L^{-1} salinity. The distiller is powered by the waste heat fluxes reported in Tab. 1, which are recovered from the coolant circuit of the electric power generator by means of the finned heat exchanger.

Operating Condition	Heat Flux, ϕ [W m^{-2}]
No Load	783.3
Half Load	933.3
Full Load	1116.7

Table 1: Heat flux between the heat exchanger (HEX) connected to the coolant circuit of the generator set (GENSET) and the passive multi-effect desalination device (LT-MD).

The measured performance of the distiller is shown in Fig. 4. The figure on the left shows the distillate flow rate (*i.e.* specific mass of freshwater produced with time) for different operating conditions of the generator set. Blue and red bars represent the experimental and modeling performance, respectively. The device produced specific mass flow rates of 1.55 ± 0.20, 1.96 ± 0.13 and 2.61 ± 0.24 L m^{-2} h^{-1} in case of no load, half load and full load, respectively. The model predictions, obtained from Eq. (13), are in good agreement with the experimental results: the predicted specific mass flow rates are 1.52 ± 0.23 (2% mismatch with respect to experiments), 1.93 ± 0.28 (1.5% mismatch) and 2.46 ± 0.32 L m^{-2} h^{-1} (5% mismatch) in case of no load, half load and full load, respectively. The error bars for the experimental results are obtained from the time series of data about freshwater yield at steady state, and error intervals are reported in terms of ± 1 standard deviation. On the other hand, the uncertainty of the model estimations is determined from the upper and lower values of the parameters that mainly affect the modeling results. In detail, the convective heat transfer coefficient h (distiller-ambient), the porosity of the hydrophobic membrane ϵ_m and the porosity of the spacer ϵ_a are ranged in the following intervals: $5 < h < 15$ W m^{-2} K^{-1}, $0.75 < \epsilon_m < 0.85$ and $0.65 < \epsilon_a < 0.75$. Note that the distillate productivity is normalized with respect to the surface of the heat exchanger, which is equivalent to that of the hydrophilic wicks (0.049 m^2).

On the right side of Fig. 4 we report the energy consumption of the tested distiller, which is defined as the ratio between the recovered waste heat flux from the coolant circuit and the produced distillate mass flow rate, namely $\phi \, J^{-1}$ (dark blue bars). Similarly, we also report the exergy consumption $\psi \, J^{-1}$ (light blue bars),
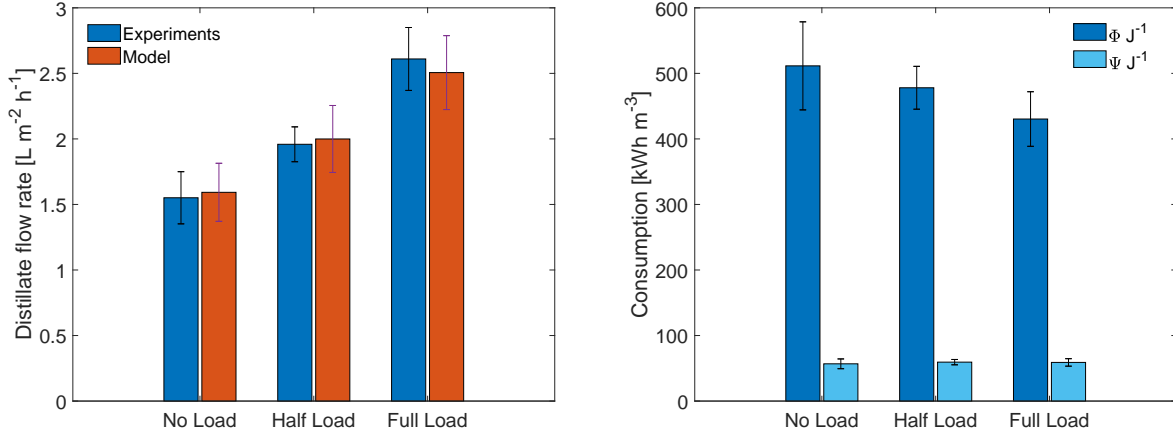
Figure 4: Desalination performance of a three-stage configuration distiller with different applied loads (see Tab. 1 for details). The picture on the left shows the modeling (red bars) and experimental (blue bars) distillate flow rates normalized with respect to the surface of the hydrophilic wicks; whilst, on the right, the energy (indicated as $\phi\ J^{-1}$, blue bars) and exergy ($\psi\ J^{-1}$, light blue bars) consumed to experimentally produce a unit volume of distillate are shown. Note that, the latter results can also be interpreted in terms of specific water production per consumed energy/exergy unit, which, for e.g. energy, yields 1.95, 2.10 and 2.32 L kWh^{-1} in case of no load, half load and full load conditions, respectively.

where the thermal exergy flux is defined as [41]

$$\psi = \phi\left(1 - \frac{T_0}{T_{TS}}\right); \qquad (15)$$

that is, the available thermal power times the Carnot efficiency. In this latter factor, T_0 is the temperature of the dead state (ambient temperature, around 23°C), and T_{TS} is the temperature of the thermal source, which is, in this case, the average between the inlet and outlet temperatures of the water-glycol mixture in the cooling circuit of the generator set (approximately 60°C, 65°C and 70°C in case of no, half and full load, respectively). The energy consumption for the three applied loads is equal to 511.47 ± 67.18, 478.03 ± 32.69 and 430.35 ± 41.66 kWh m^{-3} (corresponding to 1.95, 2.10 and 2.32 L kWh^{-1}, respectively); whilst, the exergy consumption is 56.83 ± 7.46, 59.40 ± 4.06 and 58.96 ± 5.70 kWh m^{-3}. For the sake of completeness, we remark that the quality of the obtained clean water has been checked using the refractometer and no presence of sodium chloride has been found within the instrument sensitivity.

The obtained energy and exergy consumptions are higher than the best active desalination technologies currently available on the market, e.g. around 5 kWh m^{-3} for reverse osmosis [42]. However, the proposed compact and modular device exploits a low-grade (Carnot factor around 0.13) waste heat source that would not be otherwise used, in a totally passive way and without resorting to any active component (e.g. pumps, electrovalves, etc). The thermal performance in

terms of gained output ratio, or GOR [43], is equal to 1.29, 1.37 and 1.46 in case of no load, half load and full load, respectively. It should be also noticed that the prototype has not yet been fully optimized at best in terms of materials and size, since the aim of this work is only to demonstrate a proof-of-concept of the coupling between the generator set and the passive multi-stage distiller. For these reasons, the energy and exergy consumptions will be compared with other similar waste heat driven desalination technologies in the next Section.

In Fig. 5, the temperature profile in case of full load is reported. We report both data from experiments and model. The overall thermal gradient across the stack is ≈ 25°C and the experimental results (red triangles in Fig. 5) show a good agreement with the model predictions (gray band in Fig. 5).

4.2. Model extrapolation

The validated model is then used to assess how the thickness of the air gap (*i.e.* the thickness of the spacer) and the number of stages affect the produced distillate flow rate.

Figure 6 (panel on the left) shows the distillate productivity in case of a three-stage configuration device as a function of the thickness of the air gap. This value is extremely important, and it must be chosen with care. In fact, a larger thickness leads to both a larger vapor pressure drop (positive effect for the productivity) and a lower permeability (negative effect): the optimal value
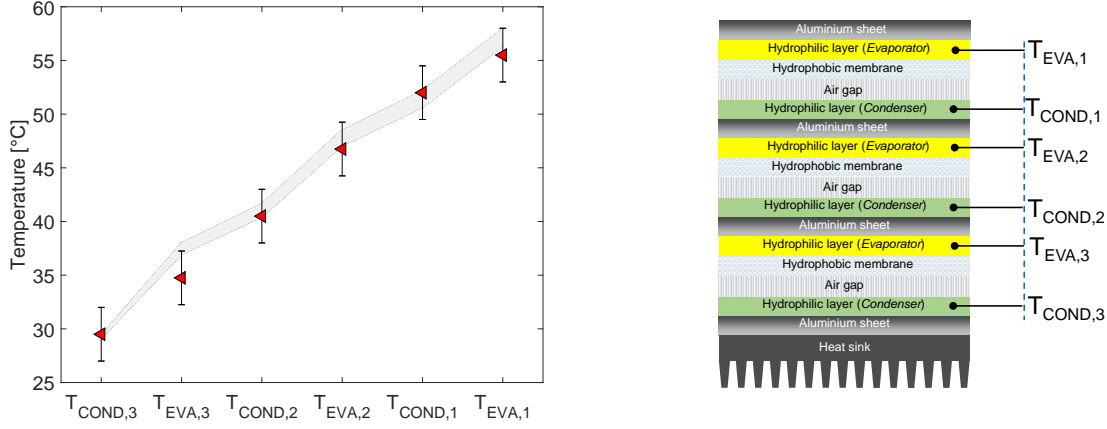
Figure 5: Temperature profile through the layers of the three-stage distiller. Full load operating conditions are considered. The gray band represents the model predictions, whilst red triangles experimental data (±1 s.d.). In the figure on the right, details on the positioning of the thermocouples in the distiller are shown.

that is found to maximize the productivity is around 1.25 mm. When the air gap is thicker than this latter value, the decrease in permeability plays a more important role as compared to the increase in temperature gradient and, as a result, the productivity starts to decrease. Note that, the commercial spacer used here (d_a equal to 1 mm, see the red point in the picture) is very close to the optimal value.

Figure 6 (panel on the right-hand side) shows the modeling predictions of the freshwater production from seawater as a function of the number of distillation stages. The model shows that, at fixed air gap thickness ($d_a = 1$ mm), the best performance is achieved by a six-stage configuration, which could produce up to 5 L m^{-2} h^{-1}. The latter productivity would allow to produce nearly 120 liters of freshwater per day by a 1 m^2 evaporating surface. Note that, the distillate flow rate scales rather linearly with the number of stages up to a critical threshold, which depends on the feed water salinity and the tested stratigraphy. In particular, increasing the number of stages beyond the critical threshold leads to a decrease in productivity. This is due to a decrease of the temperature gradient throughout the stages, which results to be less effective in counteracting the effect of the activity gradient on the vapor pressure drop Δp_v. It is worth to remark that the productivities reported in Fig. 6 are obtained under a fixed heat flux (full load conditions, namely 1.12 kW m^{-2}), which allows to distinctively determine the operating temperature of the first-stage evaporator ($T_{EVA,1}$). The latter temperature indicates that, in the current implementation, the coolant circuit could be coupled to a distiller

with up to five stages, since it can provide a thermal energy flux at temperatures lower than 80°C. Distillers with six or more stages, instead, should be coupled with a heat exchanger capable of recovering the thermal energy contained in the exhaust gases, whose temperature can be up to 500°C according to the data sheet of the generator set.

4.3. Comparison with other solutions

A comparison between the energy and exergy consumptions of the proposed desalination device, powered by the waste heat from a small-scale generator set, is carried out with respect to analogous solutions reported in the literature. The results are shown in Fig. 7. The performance is reported in terms of consumed kWh of waste heat per cubic meter of produced distilled water.

As far as our passive device (indicated as LT-MD) is concerned, we have considered the experimental (three-stage configuration; energy consumption $\approx 430.35 \pm 41.66$ kWh m^{-3}) and model extrapolation results (six-stage configuration; energy consumption $\approx 225.50 \pm 18.00$ kWh m^{-3}) achieved powering the device with 1.12 kW m^{-2}. Since, in the latter case, the required temperature in the first-stage evaporator is $\approx 94°C$, the heat exchanger is envisioned to be coupled with the circuit of the exhaust gases. The Carnot factors are ≈ 0.13 and 0.19, respectively. Then, the exergy consumptions yield $\approx 58.96 \pm 5.70$ kWh m^{-3} and $\approx 44.11 \pm 2.46$ kWh m^{-3} (see left panel of Fig. 7).

Fengming Zhang and co-workers proposed another low-temperature multi-effect desalination system (indicated as LT-MED) powered by the cooling water of a
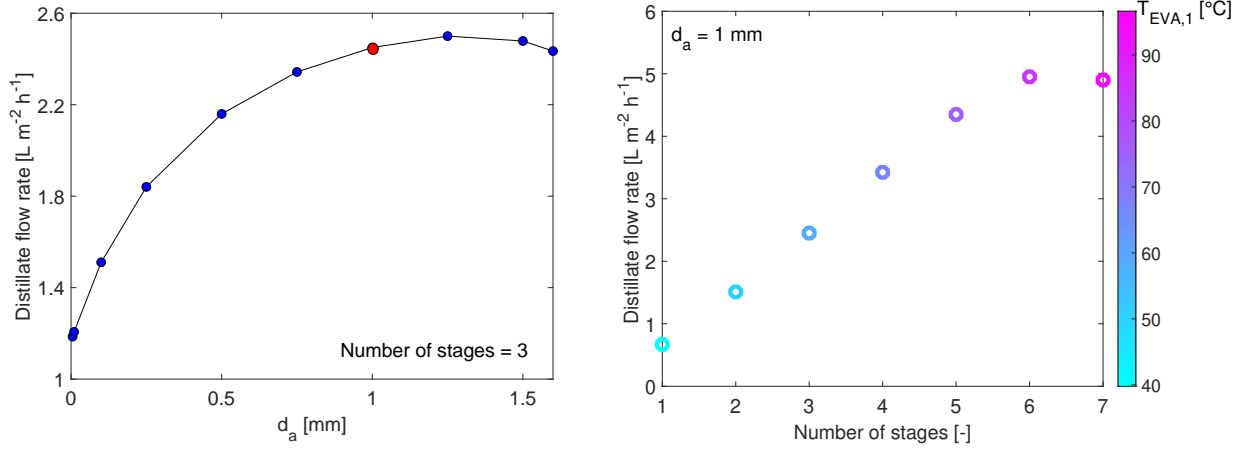
Figure 6: Modeling predictions of the distillation performance. On the left, we report the performance of a three-stage distillation device as a function of the thickness of the air gap (d_a from 5 μm to 1.65 mm), placed in series with the membrane. The red point represents the productivity obtained with the thickness used in the experimental tests (1 mm). On the right, a sensitivity analysis on the performance varying the number of distillation stages is reported (d_a = 1 mm). The different colors of the dots represent the predicted temperature of the first-stage evaporator. All estimations are carried out considering a fixed heat flux provided by the heat exchanger (full load conditions, namely 1.12 kW m^{-2}) and a feeding NaCl-water solution with 35 g L^{-1} salinity.

diesel engine [27]. It consists of 4 evaporators and 1 condenser, and the entire low-temperature evaporation process is operated under low pressure conditions generated by a vacuum pump (active technology). When the heat load of the power generator is 300 kW, the freshwater production rate is 1.26 m^3 h^{-1}, and the energy consumption is 238 kWh m^{-3}. The temperature of the recovered heat source is 47.5°C, and the resulting exergy consumption is 18.2 kWh m^{-3}.

Tanaka and co-workers [28] proposed a multi-effect diffusion still (indicated as DS) powered by the waste heat from a portable electric generator, which was recovered via a heat pipe. Two configurations are considered: the distiller tested in a vertical single-effect diffusion still (experimentally tested), and a ten-stage device (model predictions). As far as the experimental results are concerned, Tanaka and co-workers reported results for two applied loads, which led to 1857 and 2000 kWh m^{-3} energy performance (single-stage configuration). The temperatures of the recovered heat sources is 90°C (Carnot factor $\approx$ 0.18) and 145°C (Carnot factor $\approx$ 0.3), then the corresponding exergy consumptions are 369 and 541 kWh m^{-3}. On the other hand, the model prediction of the ten-stage configuration device is 226 kWh m^{-3} (temperature of the heat source not reported).

Finally, Maheswari and co-workers [44] studied a desalination device consisting of a submerged horizontal tube straight pass evaporator (indicated as SHTE) and a condensing unit. The system absorbs heat from the exhaust gases of an internal combustion engine. The ob-

served freshwater production is 0.8 and 3.0 L h^{-1} from saline water, in case of powering the desalination device with 0.92 and 3.68 kW, respectively. The resulting energy consumptions are 1148 and 1225 kWh m^{-3}, respectively. The temperatures at which the recovered heat is exchanged are 167°C and 265°C (single-stage configuration device, for which experimental data are shown). The Carnot factors are equal to 0.33 and 0.45, leading to the following exergy consumption: 376 and 551 kWh m^{-3}.

Note that, the desalination technologies powered by waste heat from small-scale generator sets proposed so far in the literature are all active (*i.e.* they involve mechanical moving parts); whereas, the solution discussed in this work is completely passive.

5. Conclusions

In this work, we have investigated the performance of a completely passive membrane distillation device when powered by low-grade heat recovered from the coolant circuit of an emergency power generator set. In-field experimental tests have shown that a three-stage configuration of the distillation device yields up to 2.61 L m^{-2} h^{-1} freshwater production from seawater when the generator set is in full load operating conditions. In perspective, a one-square-meter device could satisfy the daily clean water needs (2 liters per person per day for drinking purposes) of nearly 30 people. The extrapolations obtained with the proposed theoretical model, val-
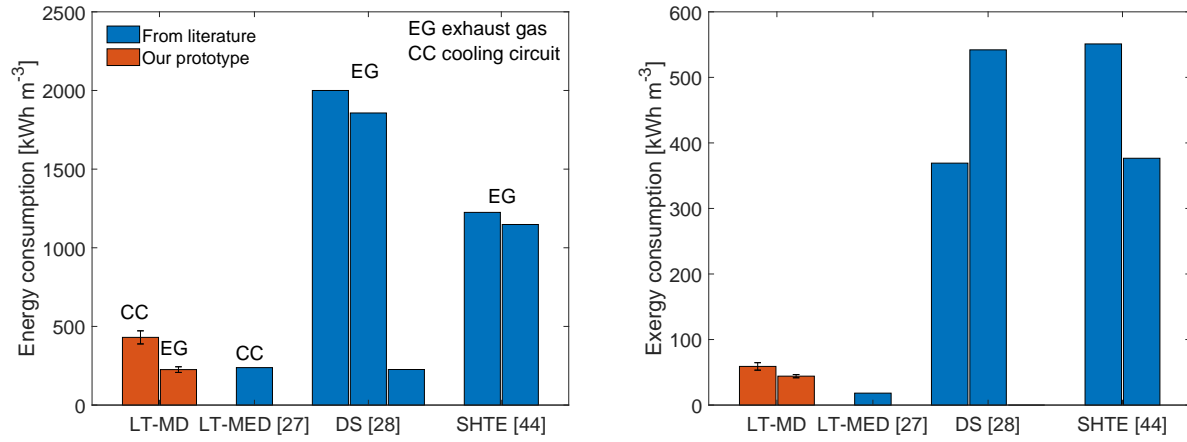
Figure 7: Comparison between performance of desalination devices powered by recovered waste heat from small-scale generator sets. The performance is expressed in terms of energy and exergy consumption to produce a unit volume of distillate (kWh m^{-3}). Red and blue bars represent the performance of our prototype and of devices from the literature, respectively. The considered desalination systems are: low-temperature multi-effect membrane distillation (LT-MD, our solution); low-temperature multi-effect distillation (LT-MED) [27]; diffusion still (DS, single and ten-stage configuration device) [28]; submerged horizontal tube straight pass evaporator (SHTE) [44]. Note that the considered devices from the literature are all active. Both couplings with exhaust gas (EG) and coolant circuit (CC) are taken into account.

idated within a 5% error on the experimental productivity, show that the concept has the potential to be further optimized.

The key aspects of the proposed solution rely on its: i) sustainability, as it allows to recover thermal energy that would otherwise be wasted to the environment, contributing to a better fuel economy; ii) robustness, thanks to the completely passive design, which does not require any mechanical moving component; and iii) low cost, thanks to the utilization of commonly available and inexpensive materials. With regards to the latter point, an assessment of the cost breakdown for the device can be obtained considering the typical price of the required items on commonly-used online wholesale markets. Considering a one-square-meter device, and a three-stage configuration, the total cost yields $\approx$ 270 USD, and includes: membranes ($\approx$ 33% of the total cost), hydrophilic layers ($\approx$ 5%), plastic air gaps ($\approx$ 2%), aluminum sheets ($\approx$ 5%) and heat sink ($\approx$ 55%). Assuming a two years life-time and continuous full load operating conditions, the cost of the produced freshwater is then estimated to be around $\approx$ 6 USD m^{-3}, which is comparable with that of other small-scale and conventional desalination technologies [6].

Therefore, the proposed coupling represents a sustainable, robust and low-cost strategy for freshwater production in off-grid and impoverished areas, where emergency power generators may be available. In perspective, the proposed device may be also directly inte-

grated into the coolant circuit of the power generators at the design stage.

Acknowledgments

References

[1] UNESCO World Water Assessment Programme, The United Nations World Water Development Report 2019: Leaving No One Behind, UNESCO, Paris, 2019.

[2] Menachem Elimelech and William A. Phillip, The future of seawater desalination: energy, technology, and the environment, Science 333 (6043) (2011) 712–717.

[3] Mesfin M. Mekonnen and Arjen Y. Hoekstra, Four billion people facing severe water scarcity, Science Advances 2 (2) (2016) e1500323.

[4] P. H. Gleick, Basic water requirements for human activities: meeting basic needs, Water international 21 (2) (1996) 83–92.

[5] S. Meunier, M. Heinrich, L. Quéval, J. A. Cherni, L. Vido, A. Darga, P. Dessante, B. Multon, P. K. Kitanidis, C. Marchand, A validated model of a photovoltaic water pumping system for off-grid rural communities, Applied Energy 241 (2019) 580–591.

[6] G. Micale, L. Rizzuti, A. Cipollina, Seawater desalination: conventional and renewable energy processes, Springer, 2009.

[7] A. Campione, L. Gurreri, M. Ciofalo, G. Micale, A. Tamburini, A. Cipollina, Electrodialysis for water desalination: A critical assessment of recent developments on process fundamentals, models and applications, Desalination 434 (2018) 121–160.

[8] N. Ghaffour, S. Lattemann, T. Missimer, K. C. Ng, S. Sinha, G. Amy, Renewable energy-driven innovative energy-efficient desalination technologies, Applied Energy 136 (2014) 1155–1165.

[9] F. Giudici, A. Castelletti, E. Garofalo, M. Giuliani, H. R. Maier, Dynamic, multi-objective optimal design and operation of water-energy systems for small, off-grid islands, Applied Energy 250 (2019) 605–616.

[10] M. Morciano, M. Fasano, U. Salomov, L. Ventola, E. Chiavazzo, P. Asinari, Efficient steam generation by inexpensive narrow gap evaporation device for solar applications, Scientific reports 7 (1) (2017) 11970.

[11] G. Ni, G. Li, S. V. Boriskina, H. Li, W. Yang, T. Zhang, G. Chen, Steam generation under one sun enabled by a floating structure with thermal concentration, Nature Energy 1 (9) (2016) 16126.

[12] T. A. Cooper, S. H. Zandavi, G. W. Ni, Y. Tsurimaki, Y. Huang, S. V. Boriskina, G. Chen, Contactless steam generation and superheating under one sun illumination, Nature communications 9 (1) (2018) 5086.

[13] P. D. Dongare, A. Alabastri, S. Pedersen, K. R. Zodrow, N. J. Hogan, O. Neumann, J. Wu, T. Wang, A. Deshmukh, M. Elimelech, et al., Nanophotonics-enabled solar membrane distillation for off-grid water purification, Proceedings of the National Academy of Sciences 114 (27) (2017) 6936–6941.

[14] P. D. Dongare, A. Alabastri, O. Neumann, P. Nordlander, N. J. Halas, Solar thermal desalination as a nonlinear optical process, Proceedings of the National Academy of Sciences (2019) 201905311.

[15] W. Wang, Y. Shi, C. Zhang, S. Hong, L. Shi, J. Chang, R. Li, Y. Jin, C. Ong, S. Zhuo, et al., Simultaneous production of fresh water and electricity via multistage solar photovoltaic membrane distillation, Nature communications 10 (1) (2019) 3012.

[16] A. Subramani, J. G. Jacangelo, Emerging desalination technologies for water treatment: a critical review, Water research 75 (2015) 164–187.

[17] P. Wang, Emerging investigator series: the rise of nano-enabled photothermal materials for water evaporation and clean water production by sunlight, Environmental Science: Nano 5 (5) (2018) 1078–1089.

[18] E. Chiavazzo, M. Morciano, F. Viglino, M. Fasano, P. Asinari, Passive solar high-yield seawater desalination by modular and low-cost distillation, Nature Sustainability 1 (12) (2018) 763.

[19] M. K. Estahbanati, M. Feilizadeh, K. Jafarpur, M. Feilizadeh, M. R. Rahimpour, Experimental investigation of a multi-effect active solar still: the effect of the number of stages, Applied energy 137 (2015) 46–55.

[20] J. Bundschuh, N. Ghaffour, H. Mahmoudi, M. Goosen, S. Mushtaq, J. Hoinkis, Low-cost low-enthalpy geothermal heat for freshwater production: Innovative applications using thermal desalination processes, Renewable and Sustainable Energy Reviews 43 (2015) 196–206.

[21] X. Wang, A. Christ, K. Regenauer-Lieb, K. Hooman, H. T. Chua, Low grade heat driven multi-effect distillation technology, International Journal of Heat and Mass Transfer 54 (25-26) (2011) 5497–5503.

[22] K. Thu, H. Yanagi, B. B. Saha, K. C. Ng, Performance analysis of a low-temperature waste heat-driven adsorption desalination prototype, International Journal of Heat and Mass Transfer 65 (2013) 662–669.

[23] V. G. Gude, Energy storage for desalination processes powered by renewable energy and waste heat sources, Applied Energy 137 (2015) 877–898.

[24] B. Rahimi, A. Christ, K. Regenauer-Lieb, H. T. Chua, A novel process for low grade heat driven desalination, Desalination 351 (2014) 202–212.

[25] H. R. Dastgerdi, P. B. Whittaker, H. T. Chua, New MED based desalination process for low grade waste heat, Desalination 395 (2016) 57–71.

[26] M. Al-Shammiri, M. Safar, Multi-effect distillation plants: state of the art, Desalination 126 (1-3) (1999) 45–59.

[27] F. Zhang, S. Xu, D. Feng, S. Chen, R. Du, C. Su, B. Shen, A low-temperature multi-effect desalination system powered by the cooling water of a diesel engine, Desalination 404 (2017) 112–120.

[28] H. Tanaka, C.-D. Park, Experimental study of distiller with heat pipe utilizing waste heat from a portable electric generator, Desalination 302 (2012) 43–49.

[29] M. Alberghini, M. Morciano, L. Bergamasco, M. Fasano, L. Lavagna, G. Humbert, E. Sani, M. Pavese, E. Chiavazzo, P. Asinari, Coffee-based colloids for direct solar absorption, Scientific reports 9 (1) (2019) 4701.

[30] Abdullah Alkhudhiri, Naif Darwish and Nidal Hilal, Membrane distillation: a comprehensive review, Desalination 287 (2012) 2–18.

[31] Jongho Lee, Tahar Laoui and Rohit Karnik, Nanofluidic transport governed by the liquid/vapour interface, Nature nanotechnology 9 (4) (2014) 317–323.

[32] Fortunato Laganà, Giuseppe Barbieri and Enrico Drioli, Direct contact membrane distillation: modelling and concentration experiments, Journal of Membrane Science 166 (1) (2000) 1–11.

[33] Theodore L. Bergman, Frank P. Incropera, David P. DeWitt and Adrienne S. Lavine, Fundamentals of heat and mass transfer, John Wiley & Sons, 2011.

[34] Bruce E. Poling, John M. Prausnitz and John P. O'connell, The properties of gases and liquids, Vol. 5, Mcgraw-hill New York, 2001.

[35] Akshay Deshmukh and Menachem Elimelech, Understanding the impact of membrane properties and transport phenomena on the energetic performance of membrane distillation desalination, Journal of Membrane Science 539 (2017) 458–474.

[36] Jongho Lee, Anthony P. Straub and Menachem Elimelech, Vapor-gap membranes for highly selective osmotically driven desalination, Journal of Membrane Science 555 (2018) 407–417.

[37] Akshay Deshmukh, Chanhee Boo, Vasiliki Karanikola, Shihong Lin, Anthony P. Straub, Tiezheng Tong, David M. Warsinger and Menachem Elimelech, Membrane distillation at the water-energy nexus: limits, opportunities, and challenges, Energy and Environmental Science 11 (5) (2018) 1177–1196.

[38] Yanbin Yun, Runyu Ma, Wenzhen Zhang, A.G. Fane and Jiding Li, Direct contact membrane distillation mechanism for high concentration nacl solutions, Desalination 188 (1-3) (2006) 251–262.

[39] J.S. Mackie and P. Meares, The diffusion of electrolytes in a cation-exchange resin membrane. ii. experimental, in: Proceedings of the Royal Society of London A: Mathematical, Physical and Engineering Sciences, Vol. 232, The Royal Society, 1955, pp. 510–518.

[40] Surapit Srisurichan, Ratana Jiraratananon and A.G. Fane, Mass transfer mechanisms and transport resistances in direct contact membrane distillation process, Journal of Membrane Science 277 (1) (2006) 186–194.

[41] A. Bejan, Advanced engineering thermodynamics, John Wiley & Sons, 2016.

[42] J. H. Lienhard, K. H. Mistry, M. H. Sharqawy, G. P. Thiel, Thermodynamics, exergy, and energy efficiency in desalination systems, Desalination Sustainability: A Technical, Socioeconomic, and Environmental Approach (2017).

[43] V. Gude, Exergy evaluation of desalination processes, ChemEngineering 2 (2) (2018) 28.

[44] K. Maheswari, K. K. Murugavel, G. Esakkimuthu, Thermal desalination using diesel engine exhaust waste heat—an experimental analysis, Desalination 358 (2015) 94–100.